Revealing Solar-Cell Photovoltage Dynamics at the Picosecond Time Scale with Time-Resolved Photoemission Spectroscopy

Y. Hazama,[1,2,*] Y. Ishida,[1] L. Zhu,[1,2,†] C. Kim,[1] S. Shin,[1] and H. Akiyama[1,2]

[1] *ISSP, University of Tokyo, Kashiwa, Chiba 277-8581, Japan*

[2] *AIST-UTokyo OPERANDO-OIL, University of Tokyo, Kashiwa, Chiba 277-8589, Japan*

(Received 10 January 2018; revised manuscript received 29 April 2018; published 25 September 2018)

The picosecond dynamics in a GaAs solar cell is studied using time-resolved photoemission spectroscopy. At a pump fluence of 0.081 μJ/cm^2, photovoltage builds up in approximately 23 ps. The subsequent decay of the voltage is found to occur over 7 ns. These quantities reflect the time scales of carrier transport and recombination, both of which are critical factors for the conversion efficiencies of solar cells. We demonstrate that the on-site properties of solar cells relevant to conversion efficiency are directly accessible with picosecond temporal resolution using the photoemission technique. Application of the present technique will open a new route in the pursuit of optimal designs for solar-cell structures.

DOI: 10.1103/PhysRevApplied.10.034056

I. INTRODUCTION

Fabrication of low-cost and highly efficient solar cells has attracted considerable research interest due to their industrial applications. In addition to silicon-based solar cells [1], various types of materials and structures have been studied, including organic [2–4], intermediate-band [5,6], dye-sensitized [7–9], and perovskite solar cells [10–13]. Advanced concepts have also been introduced to challenge the Shockley-Queisser limit [14], including photon recycling [15], carrier multiplication [16], and photonic confinement [17,18].

In addition, developing new methods for characterizing solar cells will be required. In particular, it would be interesting to reveal how the photovoltage emerges and decays after light impinges on a cell. It is believed that the photogenerated electrons and holes drift into opposite directions, which results in the generation of photovoltage; this process occurs in the pico-to-nanosecond time region. A variety of microscopic processes may also be taking place therein, such as carrier transport, recombination, and photonic effect. However, it is difficult to detect the voltaic changes in the pico-to-nanosecond time region using electronic devices because of the limitations of time resolution. For example, investigating the decay of the open-circuit photovoltage using open-circuit voltage decay (OCVD) [19–21] is one way to investigate the photovoltage dynamics, but probing subnanosecond dynamics is challenging because undesirable high-frequency responses of the electronic circuits can distort the genuine dynamics of the cells. Fast dynamics can be accessed by some optical pump-probe techniques such as the ultrafast fluorescence spectroscopy; however, photovoltage cannot be measured.

Time-resolved photoemission spectroscopy (TRPES), implemented by a femtosecond pulsed laser source, provides an opportunity to record the transient photovoltage in the pico-to-nanosecond time region. In this method, a pump pulse initiates the dynamics; subsequently, photoelectrons are ejected by the probe pulse. As the photoelectrons can feel the photovoltage, the photoelectron spectrum or the kinetic energy distribution of the photoelectrons will be shifted accordingly (Fig. 1). Although the photoelectrons consisting of the spectrum are ejected from the surface region, the photovoltage generated across the p-n junction interface, located deep in the bulk, can be monitored. TRPES has been utilized to investigate the surface photovoltage (SPV) dynamics in doped semiconductors [22–27]. Some attempts have also been made to monitor the photovoltage and charge transfer in some device structures [28,29]. However, the application of TRPES to practical solar cells has yet to be demonstrated. Herein, we apply TRPES to a GaAs solar cell. We succeed in detecting the photovoltage rise time of approximately 23 ps at a pump fluence P = 0.081 μJ/cm^2. Subsequent decay of the photovoltage occurred over approximately 7 ns. The P dependency of the buildup time is also investigated. The buildup and decay times of the solar cell's photovoltage provide a new insight into carrier transport and recombination.

II. EXPERIMENT

Figure 2(a) shows the structure of the GaAs solar cell. Samples are fabricated using a solid-source MBE system

*hazama@issp.u-tokyo.ac.jp

†Present address: Sun Yat-sen University, Higher Education Mega Center, Guangzhou 510006, China.

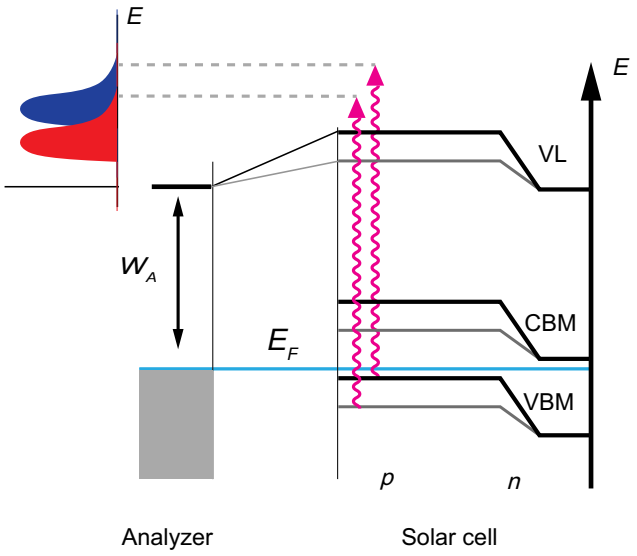

FIG. 1. Energy diagram of a solar cell in electrical contact with a photoelectron analyzer. The gray (black) curves show the energy levels in the presence (absence) of photovoltage. VL, CBM, VBM, and E_F indicate the vacuum level, the conduction band minimum, the valence band maximum, and the Fermi level, respectively. The photoelectron spectrum obtained in the presence (absence) of photovoltage is shown in red (blue).

(VG80H) equipped with standard conical effusion cells for group III elements (Ga and Al) and cracker sources for group V (As) (Veeco). Samples are prepared for growth by thermal oxide desorption under As flux at 620 °C for 20 min. A (0.2–4) $\times$ 10^{18} cm^{-3} Si-doped n^+ (100) GaAs substrate is prepared as the starting material for solid-source MBE growth of different crystalline layers of the heterostructure solar cells. After the desorption is completed, the epitaxial growth starts with a 500-nm-thick GaAs buffer layer with Si doped at 3 $\times$ 10^{18} cm^{-3}, which is grown at 580 °C with a growth rate of 1 monolayer per second (ML/s) to enhance the surface morphology and with a Ga beam source at 1014 °C. During the growth, the beam equivalent pressure of As_4 is 1 $\times$ 10^{-5} Torr. The film growth rates are determined by monitoring the intensity of the specular spot of the reflection high-energy electron diffraction pattern. All layers are grown at 580 °C at the same substrate temperature. At a GaAs growth rate of 1 μm/h, the base pressure of the MBE main chamber is 1.5 $\times$ 10^{-7} Torr. The back surface field (BSF) layer comprised a 30-period superlattice of $Al_{0.1}Ga_{0.9}As$ barriers and GaAs wells with Si doped at 3 $\times$ 10^{18} cm^{-3}. The BSF layer acts as a barrier to minority-carrier holes in the *n*-GaAs region, which increases the probability of their collection across the *p*-*n* junction. A superlattice is used for this purpose rather than just a thick $Al_xGa_{1-x}As$ region because in MBE, a GaAs region grown on a superlattice exhibits a better electrical interface than when a GaAs region is grown on a thick $Al_xGa_{1-x}As$ region. A 3-μm-thick base is grown with doped Si (2 $\times$ 10^{17} cm^{-3}), followed by an intrinsic region with a 500-nm-thick undoped GaAs layer. Then, a 660-nm-thick GaAs *p*-type emitter is grown with doped carbon (1 $\times$ 10^{18} cm^{-3}). After a 30-nm-thick *p*-type $Al_{0.66}Ga_{0.34}As$ window layer is grown with carbon doping (3 $\times$ 10^{18} cm^{-3}), an *p*-type GaAs layer with a thickness of 5 nm is epitaxially grown to provide a stable and nonoxidized surface for the solar cells.

The TRPES apparatus [30] comprised a hemispherical electron analyzer and a Ti:sapphire laser system delivering 1.5-eV pump and 5.9-eV probe pulses at 250 kHz. The time and energy resolutions are $\Delta t_{p\text{-}p} \sim 280$ fs and approximately 15 meV, respectively. The spot diameters of the pump and probe beams are 250 and 85 μm, respectively, estimated using a pin hole with a diameter of 200 μm attached next to the sample. The spatial overlap of the pump and probe beams on the sample is tuned by maximizing the TRPES signal of highly oriented pyrolytic graphite. Using the pin hole, we check that the spot of the pump beam does not move for 5 μm when the delay stage is mechanically shifted from -300 to 600 ps pump-probe delay. The pump fluence P is controlled by a combination of a polarizer and a wave plate [30] and also by some neutral density filters inserted in the optical path of the pump beam. In this way, we achieve P as small as 0.081 $\mu J/cm^2$. Note, each time we exchange the neutral density filter, we recalibrate the origin of the pump-probe delay by the graphite method. Such a recalibration is necessary because the optical path length of the pump beam line depends on the degree of the attenuation of the neutral density filter. Photoelectron spectra are obtained on the *p*-type surface of the GaAs solar cell at room temperature. We do not perform any surface cleaning before acquiring the spectrum because our interest is in the photovoltage that emerges at the *p*-*n* junction, which is detected as the voltaic shift of the spectrum on the *p*-type side of the sample. The non-necessity of the cleaning treatment increases the accessibility of the present technique to reveal the picosecond dynamics of a solar cell.

III. RESULTS AND DISCUSSION

Figure 2(b) shows the spectra obtained on the *p*-doped face of the GaAs solar-cell heterostructure. The blue curve is recorded without irradiating the pump pulses on the sample. The spectrum is tailed towards the higher kinetic energy, which is typical of a spectrum recorded on a sample without any surface-cleaning treatment, as mentioned in the previous section. The cutoff appearing in the lower kinetic energy is due to the work function. The spectrum shifts into lower kinetic energies when the sample is illuminated by the pump; see the red curve in Fig. 2(b), acquired at $t = 0$ ps. The direction of the pump-induced shift is in accord with that expected when the band bending formed across the *p*-*n* junction interface

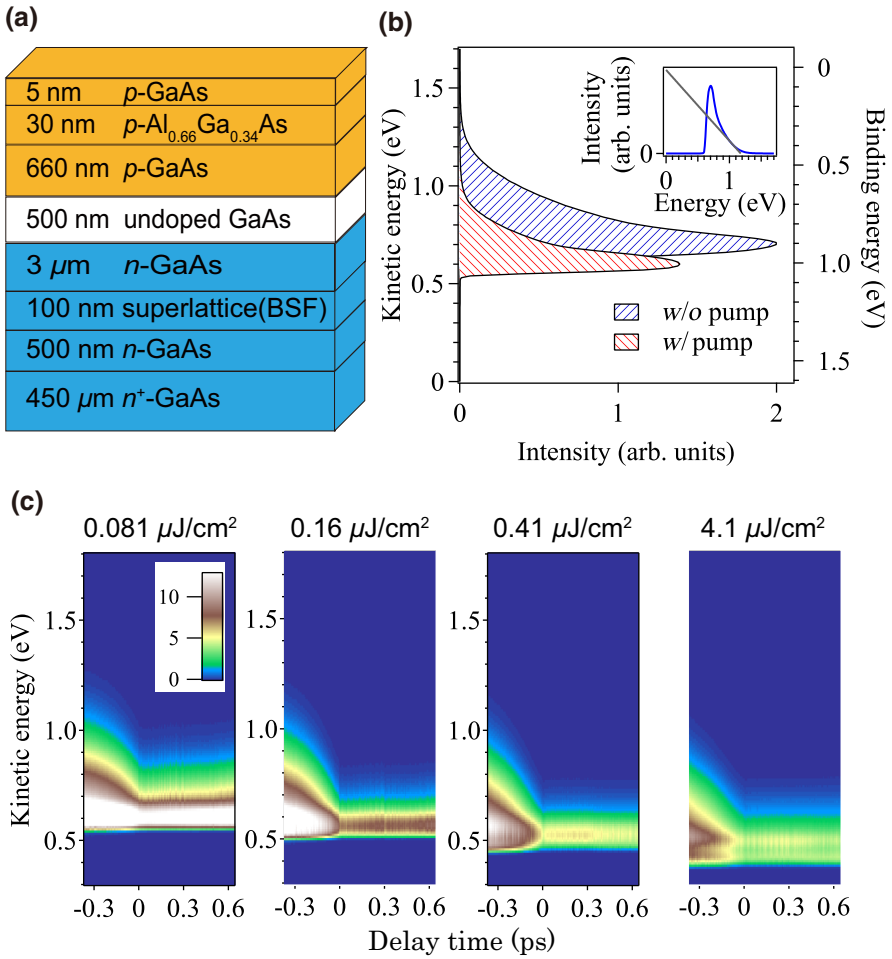

FIG. 2. GaAs solar cell and TRPES spectra. (a) Structure of the GaAs solar cell. p layers and n layers are doped with carbon and silicon, respectively. (b) Photoelectron spectra obtained at the surface of the p layer with (red) and without (blue) the pump. The former is measured at $t = 1$ ps with a pump intensity of 0.081 μJ/cm^2. The reference of the binding energy on the right vertical axis is determined by recording the Fermi cutoff of gold in electrical contact to the sample and the analyzer. The inset shows an example of linear fitting to the latter spectrum at the high-energy tail. (c) Photoemission intensities as functions of energy and delay time measured at 0.081, 0.16, 0.41, and 4.1 μJ/cm^2.

shows light-induced relaxation. Note that P is as low as 0.081 μJ/cm^2. Such a low P has not been achieved in TRPES studies of SPVs generated on the edge of semiconductive materials. For example, $P > 100$ μJ/cm^2 was adopted in the study of p-GaAs [23,31,32] to observe a similar amount of photovoltage; $P \gtrsim 10$ μJ/cm^2 was the case for the SPVs generated on bulk-insulating topological insulators [33,34]. The low fluence of 0.081 μJ/cm^2 is a measure of the high efficiency in the photovoltage generation in our solar-cell sample.

By varying the pump-probe delay, we can study the temporal evolution of the photoelectron spectra. The panels in Fig. 2(c) are maps of the photoelectron intensity in the E-t plane. The photovoltaic shift of the spectrum is seen at $t > 0$ ps. The amount of the shift increased as the pump intensity P is varied from 0.081 to 4.1 μJ/cm^2. We also observe a counterintuitive shift at $t < 0$ ps or when the pump pulse did not arrive. A similar shift at $t < 0$ ps is also observed when SPVs in semiconductors are studied by TRPES [28,32,35,36], which can be attributed to the so-called propagation effect [32,36]. We will investigate this effect later.

Next, we quantify the pump-induced shift of the spectra. To this end, we fit the high-energy tail of the spectra with a linear function and estimate the shift; see the inset in Fig. 2(b). We do not use the low-energy cutoff to evaluate the shift because the cutoff may be due to the work function of the analyzer. Figure 3 shows the extracted shift for various P as functions of t. The shift is referenced to the band edge of the spectrum recorded without the pump. The shift is maximum at approximately 0 ps, regardless of P, and diminishes toward both $t > 0$ and $t < 0$; the latter reflects the propagation effect.

Figure 4 shows the maximum shift as a function of P. The shift increases with P and saturates at approximately 0.45 V at $P \gtrsim 0.8$ μJ/cm^2. For GaAs solar cells, the open-circuit photovoltage saturates at approximately 1 V in the steady-state condition or when a constant wave light is irradiated. The smaller saturation value obtained in the present measurement may be attributed to the voltage drop caused by in-plane conduction between the illuminated area and the surroundings or to some far-from equilibrium effects such as carrier heating. We note that SPV occurring on the p-doped face of the sample is expected to play a minor

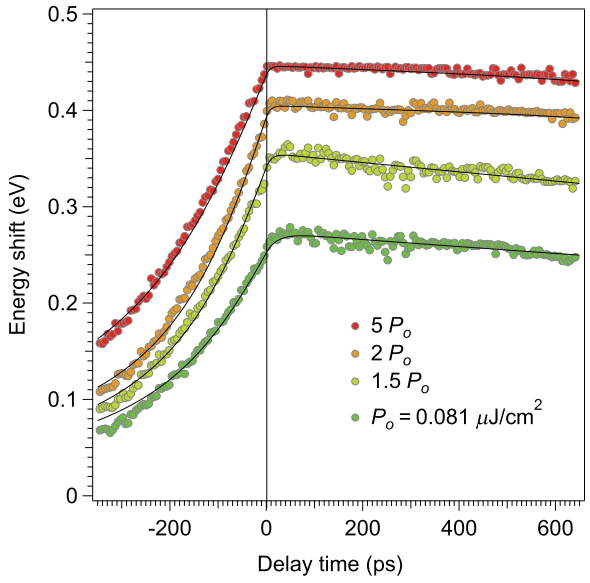

FIG. 3. Spectral shift as a function of delay time. Here, $P_0 = 0.081\ \mu\text{J/cm}^2$. Black curves show the fitting functions; see the text.

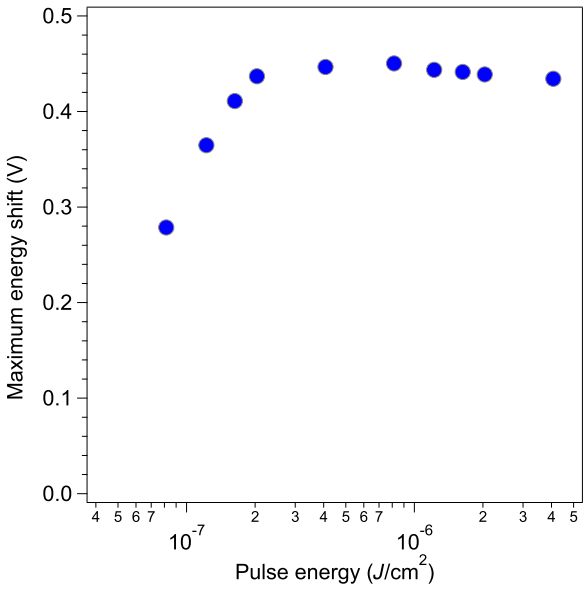

FIG. 4. The maximum energy shift of the photoemission spectra as a function of pump intensity.

role in the present condition for the following reasons: (1) The SPV on a GaAs surface is in the order of tens of millivolts [31,32] for the highest pump level in the present measurement, and reaches hundreds of millivolts only at $P > 100\ \mu\text{J/cm}^2$ [23], while such a voltaic shift is observed at the pump fluence as low as $0.081\ \mu\text{J/cm}^2$ herein; thus, the SPV shift is expected to be smaller by one to two orders of magnitude than the shift detected herein. (2) Concerning the direction of the surface band bending developed on the edge of a p-type GaAs, the SPV should shift the valence-band spectrum into higher kinetic energy, the direction of which is opposite to the observation herein. The slight decrease in the energy shift at $P > 1\ \mu\text{J/cm}^2$ may be attributed to SPV.

To extract the actual dynamics of the photovoltage, we need to separate the propagation effect from the pump-induced shift. The effect is shown schematically in Fig. 5(a). At $t < 0$ ps, photoelectrons are emitted from the p-doped layer before the photovoltage dynamics start. The photoelectrons then propagate from the sample to the analyzer. During propagation, the photoelectrons feel at most the electrostatic potential caused by the mismatch of the work functions between the analyzer and the p-doped face of the solar cell. When a pump pulse hits the sample and initiates the photovoltage dynamics, an electrostatic potential $U(r,t)$ is formed on the vacuum side to the sample surface. The typical length scale L of the potential is on the same order as the spot size of the pump beam. If the photoelectrons are still propagating within this region, their motion is affected by the time-dependent U. Thus, the kinetic energy of the photoelectrons detected by the analyzer is reduced approximately by the magnitude of U at the position wherein the electrons start to feel the photo-induced potential. In this scheme, the spectral shift at $t < 0$ ps extends to the time scale $\tau_{\text{escape}} \sim L/v$, where v is the speed of the photoelectron. We observe that the duration τ_{half} of the spectral shift at $t < 0$ ps, as characterized by the time when the shift becomes half of its maximum, is an increasing function of P; see Fig. 6. This observation is consistent with the theoretical scheme of the propagation effect described above: L and hence τ_{escape} increase when P is increased because when P is increased beyond the energy wherein the photovoltage is saturated, the area on the surface showing finite voltage increases [36].

The change in kinetic energy of a photoelectron emitted at delay time t can be expressed as

$$\Delta E(t) = \begin{cases} \int_{r(0)}^{\infty} drF[r, t_d(t)] & (t < 0), \\ \int_{0}^{\infty} drF[r, t_d(r)] & (t \geq 0). \end{cases} \quad (1)$$

Here, $F(r,t) = -(\partial U/\partial r)(r,t)$, $r(t)$, and $t_d(r)$ are the force exerted by the potential $U(r,t)$, the positon of a photoelectron at delay time t, and the delay time when the electron is at positon r, respectively. $U(r,t)$ depends on the in-plane spatial profile of photovoltage. When the profile is approximated by a uniform circle, the potential can be expressed as $U(r,t) = qV_{\text{PV}}(t)[1 - (r/\sqrt{r^2 + R_0^2})]$, where q, $V_{\text{PV}}(t)$, and R_0 are the charge of an electron, photovoltage at delay time t, and the effective radius of the area exhibiting the photovoltage, respectively [36].

To determine the rise time τ_R and the decay time τ_D of photovoltage, we fit the spectral shift assuming $V_{\text{PV}}(t) = V_0(1 - e^{-t/\tau_R})e^{-t/\tau_D}$, where V_0 is a constant. The result of

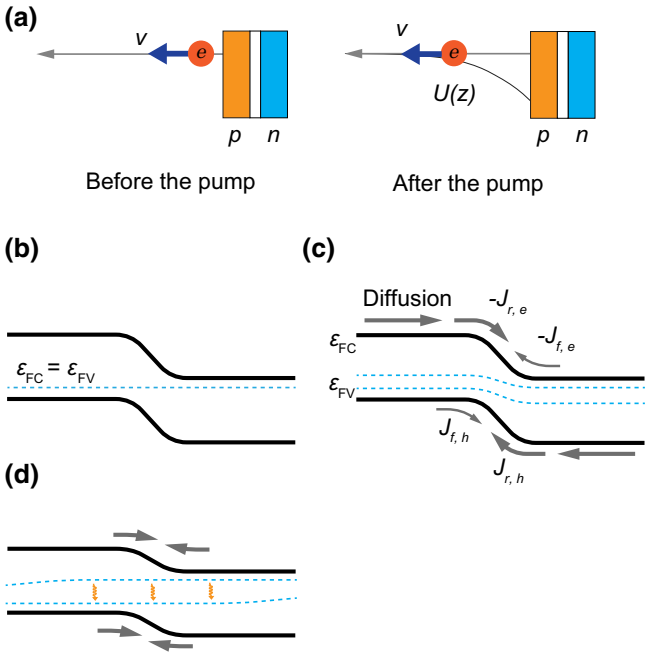

FIG. 5. (a) Schematic of a photoelectron before and after the pump. Schematic of the Fermi energy and electric current in a solar cell (b) before the pump, (c) immediately after the pump, and (d) during the decay of photovoltage.

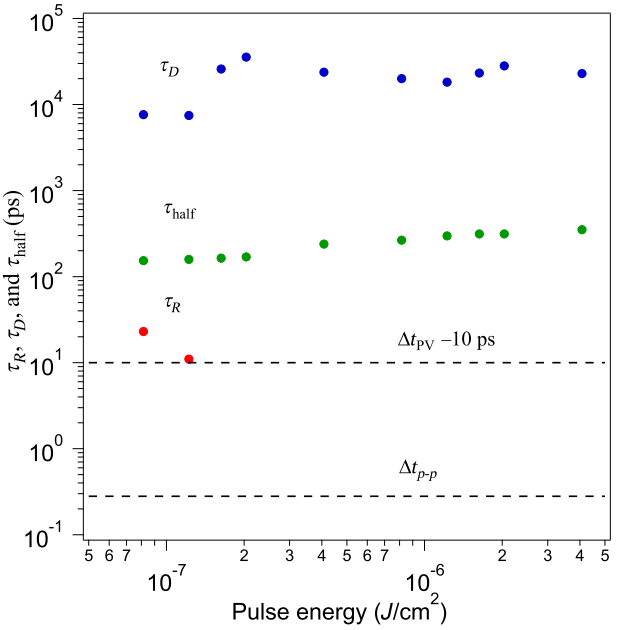

FIG. 6. τ_R, τ_D, and τ_{half} as functions of pump intensity. The temporal resolution of the pump-probe setup and the effective resolution for the extraction of τ_R are shown by broken lines. For $P > 0.12\ \mu J/cm^2$, τ_R becomes shorter, and its estimation through fitting is prevented by the slowly increasing shift at $t < 0$ ps caused by the propagation effect.

the fitting is shown by the black curves in Fig. 3. τ_R and τ_D extracted by the fitting are plotted in Fig. 6 as functions of P. The rise time is approximately 23 ps at 0.081 $\mu J/cm^2$. For higher P, the rise time becomes shorter than $\Delta t_{PV} \sim$ 10 ps, and it is difficult to extract the rise time through the fit because of the propagation effect.

The rise time of photovoltage is determined by diffusion and charge separation of minority carriers. As shown in Fig. 5(b), the quasi-Fermi-energy of the conduction and valence band, ε_{FC} and ε_{FV}, are equal and uniform in the solar cell before photoexcitation. When the pump pulse excites the sample, minority carriers are generated in both the p and n layers, which causes a mismatch between ε_{FC} and ε_{FV}. In addition, both quasi-Fermi-energies are no longer uniform between the p and n layers [see Fig. 5(c)]. Electrons (holes) then diffuse in the p (n) layer and those that reach the depletion region are quickly transferred to the opposite layer because of built-in electric field causing an electric current $J_{r,e}$ ($J_{r,h}$) of electrons (holes) in the reverse direction. As the transfer develops, charges are accumulated at the edge of the depletion region. Accordingly, the built-in electric potential is weakened, and a current $J_{f,e}$ ($J_{f,h}$) in the forward direction builds up. $J_f = J_{f,e} + J_{f,h}$ then balances $J_r = J_{r,e} + J_{r,h}$ at a point, and the net current $J_{tot} = J_f + J_r$ becomes zero. Photovoltage reaches its maximum at this point because minority carriers do not further accumulate at the edge of the depletion region. Then, the photovoltage gradually decreases because of the recombination of carriers, as shown in Fig. 5(d).

Therefore, the rise time of photovoltage corresponds to the time scale in which the accumulation of minority carriers at the edge of the depletion region is completed. The decrease in τ_R for higher pump intensities thus indicates that the charge accumulation develops faster because of the larger J_r. Note that J_r can be influenced by the motion of minority carriers in both the p (n) layer and the depletion region. In the present case, the built-in electric field in the depletion region is $E_b \sim 20$ kV/cm assuming a built-in electric potential $V_b \sim 1$ V. At this field strength, the drift velocity v_d of an electron is expected to no longer be proportional to electric field because of the scattering of electrons from Γ to L and X valley. In other words, the relationship $v_d = \mu_e E_b$ does not hold, where μ_e represents electron mobility. According to Ref. [37], v_d under this field strength takes the value of approximately 1×10^5 m/s. It thus takes approximately 5 ps for the electron to pass the depletion region. Therefore, the longer rise time of $\tau_R \sim 23$ ps at 0.081 $\mu J/cm^2$ reflects the diffusion of minority carriers in the p and n layers. However, suppression of the propagation effect is required to evaluate carrier diffusion more quantitatively because such information is reflected more directly at the early stage of photovoltage buildup, where J_r dominates over J_f and thus $J_{tot} \sim J_r$ holds.

τ_D is found to be approximately 7 ns at 0.081 μJ/cm^2. After the quasi-Fermi-energy becomes flat, ε_{FC} and ε_{FV} approach each other because of the recombination of carriers, as shown in Fig. 5(d). Therefore, the observed decay time corresponds directly to the carrier lifetime in the solar cell. Previously, the carrier lifetime in solar cells relevant to V_{oc} degradation could not be determined directly if it was shorter than the time scale accessible with OCVD. The present method thus offers a unique opportunity to obtain the on-site carrier lifetime of solar cells composed of highly absorptive materials wherein carrier lifetime is in the order of nanoseconds to picoseconds.

IV. CONCLUSION

In conclusion, we demonstrate that the picosecond dynamics of photovoltage in a solar cell can be probed by time-resolved photoemission spectroscopy. The rise time of photovoltage is determined to be approximately 23 ps at a pump intensity of 0.081 μJ/cm^2. For higher pump intensities, the rise time becomes shorter, indicating faster accumulation of carriers at the edge of the depletion region. The decay time of photovoltage that corresponds to carrier lifetime is found to be approximately 7 ns at the same pump intensity. Our study introduces a new methodology that will enable on-site studies on the diffusion of minority carriers as well as carrier lifetime in solar cells. Because these properties directly affect the conversion efficiency of solar cells, the present technique will benefit the conquest for low-cost and high-efficiency photovoltaic devices.

ACKNOWLEDGMENTS

This work is supported by NEDO in Japan, and also by KAKENHI Grant No. 18H01148.

[1] M. A. Green, Y. Hishikawa, W. Warta, E. D. Dunlop, D. H. Levi, J. Hohl-Ebinger, and A. W. H. Ho-Baillie, Solar cell efficiency tables (version 50), Prog. Photovoltaics **25**, 668 (2017).

[2] N. S. Sariciftci, L. Smilowitz, A. J. Heeger, and F. Wudl, Semiconducting polymers (as donors) and buckminsterfullerene (as acceptor): Photoinduced electron transfer and heterojunction devices, Synth. Met. **59**, 333 (1993).

[3] G. Yu, J. Gao, J. C. Hummelen, F. Wudl, and A. J. Heeger, Polymer photovoltiac cells: Enhanced efficiencies via a network of internal donor-acceptor heterojunctions, Science **270**, 1789 (1995).

[4] J. J. M. Halls, C. A. Walsh, N. C. Greenham, E. A. Marseglia, R. H. Friend, S. C. Moratti, and A. B. Holmes, Efficient photodiodes from interpenetrating polymer networks, Nature **376**, 498 (1995).

[5] M. Wolf, Limitations and possibilities for improvement of photovoltaic solar energy converters: Part I: Considerations for earth's surface operation, Proc. IRE **48**, 1246 (1960).

[6] A. Luque, A. Mart, C. Stanley, N. López, L. Cuadra, D. Zhou, J. L. Pearson, and A. McKee, General equivalent circuit for intermediate band devices: Potentials, currents and electroluminescence, J. Appl. Phys. **96**, 903 (2004).

[7] B. O'Regan and M. Grätzel, A low-cost, high-efficiency solar cell based on dye-sensitized colloidal TiO_2 films, Nature **353**, 737 (1991).

[8] N. Robertson, Optimizing dyes for dye-sensitized solar cells, Angew. Chem., Int. Ed. **45**, 2338 (2006).

[9] G. Oskam, B. V. Bergeron, G. J. Meyer, and P. C. Searson, Pseudohalogens for dye-sensitized TiO_2 photoelectrochemical cells, J. Phys. Chem. B **105**, 6867 (2001).

[10] A. Kojima, K. Teshima, T. Miyasaka, and Y. Shirai, in *210th ECS Meeting, Cancun, Mexico, Oct. 29–Nov. 3, 2006*.

[11] A. Kojima, K. Teshima, Y. Shirai, and T. Miyasaka, Organometal halide perovskites as visible-light sensitizers for photovoltaic cells, J. Am. Chem. Soc. **131**, 6050 (2009).

[12] H. Kim, C. Lee, J. Im, K. Lee, T. Moehl, A. Marchioro, S. Moon, R. Humphry-Baker, J. Yum, J. E. Moser, M. Grätzel, and N. Park, Lead iodide perovskite sensitized all-solid-state submicron thin film mesoscopic solar cell with efficiency exceeding 9%, Sci. Rep. **2**, 591 (2012).

[13] M. M. Lee, J. Teuscher, T. Miyasaka, T. N. Murakami, and H. J. Snaith, Efficient hybrid solar cells based on meso-superstructured organometal halide perovskites, Science **338**, 643 (2012).

[14] W. Shockley and H. J. Queisser, Detailed balance limit of efficiency of p-n junction solar cells, J. Appl. Phys. **32**, 510 (1961).

[15] O. D. Miller, E. Yablonovitch, and S. R. Kurtz, Strong internal and external luminescence as solar cells approach the Shockley-Queisser limit, IEEE J. Photovoltaics **2**, 303 (2012).

[16] M. C. Hanna and A. J. Nozik, Solar conversion efficiency of photovoltaic and photoelectrolysis cells with carrier multiplication absorbers, J. Appl. Phys. **100**, 074510 (2006).

[17] E. Yablonovitch and G. D. Cody, Intensity enhancement in textured optical sheets for solar cells, IEEE Trans. Electron Devices **29**, 300 (1982).

[18] L. Zeng, Y. Yi, C. Hong, J. Liu, N. Feng, X. Duan, L. C. Kimerling, and B. A. Alamariu, Efficiency enhancement in Si solar cells by textured photonic crystal back reflector, Appl. Phys. Lett. **89**, 111111 (2006).

[19] J. E. Mahan, T. W. Ekstedt, R. I. Frank, and R. Kaplow, Measurement of minority carrier lifetime in solar cells from photo-induced open-circuit voltage decay, IEEE Trans. Electron Devices **26**, 733 (1979).

[20] A. Zaban, M. Greenshtein, and J. Bisquert, Determination of the electron lifetime in nanocrystalline dye solar cells by open-circuit voltage decay measurements, ChemPhysChem **4**, 859 (2003).

[21] A. Baumann, K. Tvingstedt, M. C. Heiber, S. Väth, C. Momblona, H. J. Bolink, and V. Dyakonov, Persistent photovoltage in methylammonium lead iodide perovskite solar cells, APL Mater. **2**, 081501 (2014).

[22] M. Marsi, M. E. Couprie, L. Nahon, D. Garzella, T. Hara, R. Bakker, M. Billardon, A. Delboulbe, G. Indlekofer,

and A. Taleb-Ibrahimi, Surface states and space charge layer dynamics on Si(111)2 × 1: A free electron laser-synchrotron radiation study, Appl. Phys. lett. **70**, 895 (1997).

[23] P. Siffalovic, M. Drescher, and U. Heinzmann, Femtosecond time-resolved core-level photoelectron spectroscopy tracking surface photovoltage transients on p-GaAs, Europhys. Lett. **60**, 924 (2002).

[24] A. Melzer, D. Kampa, J. Wang, and T. Fauster, Time-resolved photoemission at the Si(100)-Ga surface using a femtosecond higher-harmonic laser source, Phys. Rev. B **80**, 205424 (2009).

[25] B. F. Spencer, D. M. Graham, S. J. O. Hardman, E. A. Seddon, M. J. Cliffe, K. L. Syres, A. G. Thomas, S. K. Stubbs, F. Sirotti, M. G. Silly, P. F. Kirkham, A. R. Kumarasinghe, G. J. Hirst, A. J. Moss, S. F. Hill, D. A. Shaw, S. Chattopadhyay, and W. R. Flavell, Time-resolved surface photovoltage measurements at *n*-type photovoltaic surfaces: Si(111) and ZnO(10$\bar{1}$0), Phys. Rev. B **88**, 195301 (2013).

[26] M. Ogawa, S. Yamamoto, K. Fujikawa, R. Hobara, R. Yukawa, Sh. Yamamoto, S. Kitagawa, D. Pierucci, M. G. Silly, C.-H. Lin, R.-Y. Liu, H. Daimon, F. Sirotti, S.-J. Tang, and I. Matsuda, Relaxations of the surface photovoltage effect on the atomically controlled semiconductor surfaces studied by time-resolved photoemission spectroscopy, Phys. Rev. B **88**, 165313 (2013).

[27] R. Yukawa, S. Yamamoto, K. Ozawa, M. Emori, M. Ogawa, Sh. Yamamoto, K. Fujikawa, R. Hobara, S. Kitagawa, H. Daimon, H. Sakama, and I. Matsuda, Electron-hole recombination on ZnO(0001) single-crystal surface studied by time-resolved soft X-ray photoelectron spectroscopy, Appl. Phys. Lett. **105**, 151602 (2014).

[28] D. Lim and R. Haight, In situ photovoltage measurements using femtosecond pump-probe photoelectron spectroscopy and its application to metal–HfO_2–Si structures, J. Vac. Sci. Technol., A **23**, 1698 (2005).

[29] B. F. Spencer, M. J. Cliffe, D. M. Graham, S. J. O. Hardman, E. A. Seddon, K. L. Syres, A. G. Thomas, F. Sirotti, M. G. Silly, J. Akhtar, P. O'Brien, S. M. Fairclough, J. M. Smith, S. Chattopadhyay, and W. R. Flavell, Dynamics in next-generation solar cells: Time-resolved surface photovoltage measurements of quantum dots chemically linked to ZnO(10$\bar{1}$0), Faraday Discuss. **171**, 275 (2014).

[30] Y. Ishida, T. Togashi, K. Yamamoto, M. Tanaka, T. Kiss, T. Otsu, Y. Kobayashi, and S. Shin, Time-resolved photoemission apparatus achieving sub-20-meV energy resolution and high stability, Rev. Sci. Instrum. **85**, 123904 (2014).

[31] S. Tokudomi, J. Azuma, K. Takahashi, and M. Kamada, Ultrafast time dependence of surface photo-voltage effect on *p*-type GaAs (100) surface, J. Phys. Soc. Jpn. **77**, 014711 (2008).

[32] S.-L. Yang, J. A. Sobota, P. S. Kirchmann, and Z.-X. Shen, Electron propagation from a photo-excited surface: Implications for time-resolved photoemission, Appl. Phys. A: Mater. Sci. Process. **116**, 85 (2014).

[33] Y. Ishida, T. Otsu, T. Shimada, M. Okawa, Y. Kobayashi, F. Iga, T. Takabatake, and S. Shin, Emergent photovoltage on SmB 6 surface upon bulk-gap evolution revealed by pump-and-probe photoemission spectroscopy, Sci. Rep. **5**, 8160 (2015).

[34] M. Neupane, S. Xu, Y. Ishida, S. Jia, B. M. Fregoso, C. Liu, I. Belopolski, G. Bian, N. Alidoust, T. Durakiewicz, V. Galitski, S. Shin, R. J. Cava, and M. Z. Hasan, Gigantic Surface Lifetime of an Intrinsic Topological Insulator, Phys. Rev. Lett. **115**, 116801 (2015).

[35] W. Widdra, D. Bröcker, T. Gießel, I. V. Hertel, W. Krüger, A. Liero, F. Noack, V. Petrov, D. Pop, P. M. Schmidt, R. Weber, I. Will, and B. Winter, Time-resolved core level photoemission: Surface photovoltage dynamics of the SiO_2Si (100) interface, Surf. Sci. **543**, 87 (2003).

[36] S. Tanaka, Utility and constraint on the use of pump-probe photoelectron spectroscopy for detecting time-resolved surface photovoltage, J. Electron Spectrosc. Relat. Phenom. **185**, 152 (2012).

[37] O. Madelung, U. Rössler, and M. Schulz, eds., *Gallium Arsenide (*GaAs*), Electron Drift Velocity and Diffusion Coefficient: Group V Elements, IV-IV and III-V Compounds. Part b - Electronic, Transport, Optical and Other Properties. Landolt-Börnstein - Group III Condensed Matter (Numerical Data and Functional Relationships in Science and Technology)* (Springer-Verlag, Berlin, Heidelberg (2017), Vol. 41A1b.